Quantum Speed Limit in Quantum Sensing

K. Herb[1,*] and C. L. Degen[1,2,†]
[1]Department of Physics, ETH Zürich, 8093 Zürich, Switzerland
[2]Quantum Center, ETH Zürich, 8093 Zürich, Switzerland

(Received 29 May 2024; accepted 11 October 2024; published 19 November 2024)

Quantum sensors capitalize on advanced control sequences for maximizing sensitivity and precision. However, protocols are not usually optimized for temporal resolution. Here, we establish the limits for time-resolved sensing of dynamical signals using qubit probes. We show that the best possible time resolution is closely related to the quantum speed limit (QSL), which describes the minimum time needed to transform between basis states. We further show that a composite control sequence consisting of two phase-shifted pulses reaches the QSL. Practical implementation is discussed based on the example of the spin-1 qutrit of a nitrogen-vacancy center in diamond.

DOI: 10.1103/PhysRevLett.133.210802

The energy-time uncertainty principle introduced by Heisenberg is a fundamental concept of quantum mechanics. While formulated loosely in Heisenberg's initial work, Robertson [1] and Bohr [2] put it on firm ground by formalizing the relationship between uncertainty and noncommutativity of observables. Twenty years later, Mandelstam and Tamm [3] showed that the energy-time uncertainty is not an uncertainty relation due to noncommutativity, but rather a statement about intrinsic timescales of quantum systems [4]. This insight led to the derivation of a quantum speed limit (QSL). To do so, Mandelstam and Tamm used the von Neumann equation with the projection operator to develop an expression for the overlap between the initial state $|\psi(0)\rangle$ and the time-evolved state $|\psi(t)\rangle$, yielding

$$\langle\psi(0)|\psi(t)\rangle \geq \cos\left(\frac{\langle\Delta H\rangle t}{\hbar}\right), \tag{1}$$

in the domain $0 \leq t \leq t_{\mathrm{QSL}}^{(\mathrm{MT})}$ where $\langle\Delta H\rangle^2 = \langle H^2\rangle - \langle H\rangle^2$ is the variance of the Hamiltonian. The minimum time needed to obtain a fully orthogonal state, i.e., $\langle\psi(0)|\psi(t)\rangle = 0$, is then given by

$$t \geq t_{\mathrm{QSL}}^{(\mathrm{MT})} = \frac{\pi}{2}\frac{\hbar}{\langle\Delta H\rangle}. \tag{2}$$

Later, Margolus and Levitin [5] proposed an alternative route to deriving a QSL based on the integrability of the Schrödinger equation to obtain a maximum evolution speed, resulting in

$$t \geq t_{\mathrm{QSL}}^{(\mathrm{ML})} = \frac{\pi}{2}\frac{\hbar}{\langle H\rangle}. \tag{3}$$

In contrast to the Mandelstam-Tamm definition, Eq. (3) bounds the time on the mean energy $\langle H\rangle$ defined relative to the energy of the ground state. For a two-level system, the two QSLs coincide while for systems open to a continuum of states or for systems consisting of more than two states, such as qutrits [6], the unified bound is tight [7,8].

Since the initial formulations of the QSL, theoretical work has focused on more complex situations such as open quantum systems [9] and systems with quantum entanglement [10], as well as applications in quantum information processing [11]. Here, the QSL sets the maximum speed at which computations can be performed and therefore permits deriving an upper bound of the computational limits of the universe [12,13]. Further, the QSL has been studied in the field of quantum optimal control [14], quantum thermodynamics [15], and metrology with respect to quantum clocks [16]. Obviously, the finite time of qubit operations will also limit the time resolution achievable in quantum sensing tasks [17]. The time limitation is of practical importance because of the many existing and envisioned applications of quantum sensors.

In this work, we investigate the relation between the QSL and the time resolution achievable in quantum sensing experiments. We show that a composite pulse sequence consisting of two phase-shifted control rotations, equivalent to a Ramsey sequence with zero time delay, reaches the QSL. Opposite to a Ramsey interferometry measurement, however, phase accumulation occurs *during* control rotations rather than a free evolution interval. We derive quantitative expressions for the quantum phase pickup as a function of control rotation angle and velocity. We use these expressions to define the time resolution and bandwidth of the sensing sequence. We also show that time

*Contact author: science@rashbw.de
†Contact author: degenc@ethz.ch

resolution can be extended beyond the QSL by trading for a reduced signal-to-noise ratio. As an example, we simulate the expected response for a nitrogen-vacancy (NV) center in diamond that is exposed to rapidly varying magnetic signal.

The canonical quantum sensing scheme of Ramsey interferometry is shown in Fig. 1(a) [17,18]. In its most basic form, the scheme uses two state transformations to initiate and halt the coherent evolution of a probe qubit subject to an external signal. The first transformation rotates the qubit from a known initial basis state $|\psi(0)\rangle = |0\rangle$ into a coherent superposition state $(1/\sqrt{2})(|0\rangle + |1\rangle)$, which then evolves for a given time τ into state $(1/\sqrt{2})(|0\rangle + e^{-i\phi(\tau)}|1\rangle)$, thereby acquiring a quantum phase

$$\phi = \int_0^\tau [\omega_0 + \delta\omega(t')]\mathrm{d}t'. \tag{4}$$

Here, $\hbar\omega_0$ is the static energy gap between the qubit's energy levels, and $\hbar\delta\omega(t)$ accounts for a small, time-dependent modulation due to the presence of the signal. After coherent evolution, a second state transformation rotates the qubit back to the original basis, followed by projective state readout [19]. By this, the canonical quantum sensing experiment measures the expectation value of the projector onto the initial state $|0\rangle$. The state transformations can be described by two control rotations, $\hat{R}$ and $\hat{R}'$, respectively. These are analogous to the start and stop triggers in a classical test and measurement task [Fig. 1(b)]. There, the time elapsed between start and stop events determines the time resolution.

Ideally, the control rotations $\hat{R}$ and $\hat{R}'$ are infinitely fast [Fig. 1(c)]. However, owing to the QSL, $\hat{R}$ and $\hat{R}'$ must have a finite duration t_R or, equivalently, a finite angular velocity (Rabi frequency Ω). In experiments, the maximum Ω may be limited by many factors, including finite available driving power, competition between ω_0 and Ω, excitation of further lying energy levels, or a combination of those. The finite speed of control rotations fundamentally limits the time resolution of the sensing sequence.

For finite t_R, qubit evolution under the signal Hamiltonian already occurs during the control rotations. The qubit-acquired phase then becomes the sum of the phase pickup during the free evolution interval and the phase pickup during control rotations [Fig. 1(d)]. In the most extreme case, the free evolution time is zero, and phase pickup occurs entirely during control rotations [Fig. 1(e)]. In this situation, the time resolution of the sequence reaches that of the QSL defined by Eqs. (2) and (3). (Note that for a qubit system, the two definitions are equivalent.)

We next derive quantitative relationships between the phase pickup ϕ_{eff}, the velocity Ω, and the angle α of control rotations. For our derivation, we focus on a bipartite control sequence consisting of two consecutive qubit rotations $\hat{R} = \hat{R}^{\alpha}_{Y}$ and $\hat{R}' = \hat{R}^{\alpha}_{\pm X}$ of equal duration t_R [Fig. 1(e)]. Here, X and Y are orthogonal axes, as shown in Fig. 1(f). This sequence represents the basic Ramsey scheme with zero time delay. The sequence duration is $\tau = 2t_R = \alpha/\Omega$, where Ω is the maximum allowed rotation velocity. In the Supplemental Material [20], we show that an equal time share ($t_R = t_{R'}$) between the two parts of the bipartite pulse sequence yields optimum sensitivity [as defined by Eq. (8) below]. This is also true when varying the angle between rotation axes.

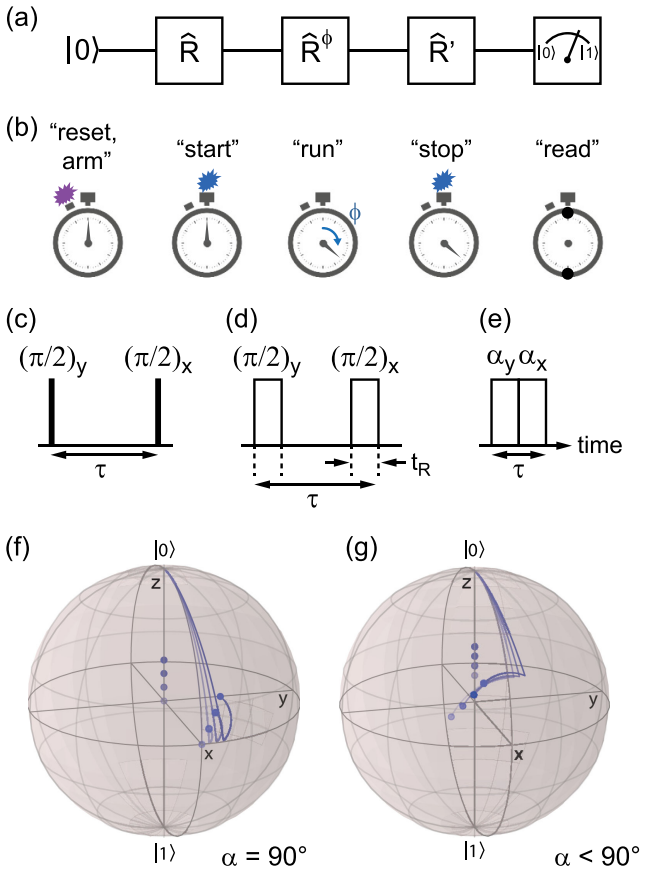

FIG. 1. Concept of time-resolved sensing at the QSL. (a) Canonical control sequence for signal estimation via quantum phase accumulation. $\hat{R}$ and $\hat{R}'$ are control rotations, and $\hat{R}^{\phi}$ is the qubit rotation due to interaction with the signal. (b) Stopwatch analogy of (a). (c) Pulse-timing diagram of the control sequence for infinitely fast control rotations. Phase accumulation occurs entirely during the free evolution time τ. $\pi/2$ are rotation angles and x, $-y$ are axes of rotation. (d) Pulse-timing diagram for finite duration $t_R > 0$ of control rotations. (e) Pulse-timing diagram at the QSL, when the interpulse delay becomes zero and $\tau = 2t_R$. Phase accumulation now occurs entirely *during* control rotations. α is the rotation angle. (f) Bloch sphere trajectories for sequence (e) with $\alpha = 90°$. Dots are the projection on the z axis. Trajectories are shown for $\phi = 0°$ (light blue), 10°, 20°, and 30° (dark blue). (g) Bloch sphere trajectories for $\alpha = 63°$. Further trajectories are shown in [20].

Our sensor output is the overlap between the initial qubit state $|\psi(0)\rangle = |0\rangle$ and the final qubit state $|\psi(\tau)\rangle$, given by the transition probability [10,17]

$$p = 1 - |\langle 0|\psi(\tau)\rangle|^2 \tag{5a}$$

$$= 1 - |\langle 0|\hat{R}\hat{R}'|0\rangle|^2 \tag{5b}$$

$$= 1 - |\langle 0|\hat{R}^{\alpha}_{\pm X}\hat{R}^{\alpha}_{Y}|0\rangle|^2. \tag{5c}$$

In the limit of strong control fields ($\Omega \gg \delta\omega(t)$), within linear response ($\phi \ll \pi/2$), and assuming that $\delta\omega(t) \approx \delta\omega$ is stationary during τ, the transition probability of this sequence is [20]

$$p = \underbrace{\frac{1}{4}(1 - \cos 2\alpha)}_{p_0} + \underbrace{\frac{1}{2}\frac{\sin\alpha(\cos\alpha - 1)}{\alpha}\phi}_{\delta_p}. \tag{6}$$

Here, p_0 is the bias point of the measurement, and δp is the change in probability due to the presence of the signal $\delta\omega$ [17]. Equation (6) defines an effective phase

$$\delta p = \frac{1}{2}\phi_{\text{eff}} = \frac{1}{2}\frac{\sin\alpha(\cos\alpha - 1)}{\alpha}\phi \coloneqq \frac{1}{2}\epsilon\phi \tag{7}$$

that corresponds to the ideal Ramsey phase $\phi = \delta\omega\tau$ [Eq. (4)] reduced by the scaling factor $\epsilon < 1$. Using Eq. (7), we can define the sensitivity η of the sequence by

$$\eta \coloneqq d[\delta p]/d[\delta\omega], \tag{8}$$

taken in the limit $\delta\omega \to 0$.

For the canonical case of qubit rotations between orthogonal axes on the Bloch sphere ($\alpha = 90°$), the transition probability is

$$p = \frac{1}{2} + \frac{\phi}{\pi}, \tag{9}$$

corresponding to $p_0 = 0.5$ and $\epsilon = 2/\pi \approx 0.637$. Figures 1(f) and 1(g) show Bloch-sphere trajectories for $\alpha = 90°$ and $\alpha < 90°$, and Fig. 2 plots ϕ_{eff} as a function of τ.

Having established the phase pick-up of the bipartite control sequence, we proceed to the problem of sampling a time-dependent signal. As a generic example, we consider the detection of a transient magnetic field $\vec{B}(t)$ using a spin-1/2 system as the qubit probe, where $\delta\omega(t) = \gamma B(t)$. Here, γ is the transduction factor (given by the gyromagnetic ratio), and $B(t)$ is the vector component of $\vec{B}(t)$ parallel to the quantization axis of the spin qubit. The influence of off-axis components of $\vec{B}(t)$ is discussed in [20].

To record a time transient, we sample $B(t)$ point by point by incrementing the delay time t of the control sequence with respect to a common start trigger at $t = 0$ [Fig. 3(a)]. For signals that vary only slowly with time, $B(t)$ is almost stationary during control pulses, and the sensor output $\delta p(t) = \epsilon\tau\gamma B(t)$ is directly proportional to the signal field. On the other hand, for more rapidly changing signals, the acquired quantum phase becomes a more complex function of signal and control fields. In a general case, we express the transition probability δp by the convolution

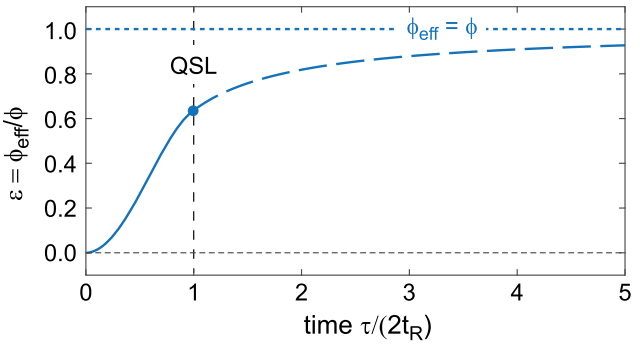

FIG. 2. Phase pickup ϕ_{eff}/ϕ as a function of τ for control rotations with finite velocity. For durations shorter than the QSL ($\tau < 2t_R$, solid curve), ϕ_{eff} is determined by the sequence of Fig. 1(e). For durations longer than the QSL ($\tau > 2t_R$, dashed curve) ϕ_{eff} is determined by the sequence of Fig. 1(d). The upper bound ($\phi_{\text{eff}} = \phi$, dotted line) is for the hypothetical case of infinitely fast control rotations, corresponding to the sequence in Fig. 1(c).

$$\delta p(t) = \int_{t'=-\infty}^{\infty} k(t' - t)\gamma B(t')\mathrm{d}t', \tag{10}$$

where $k(t)$ is the *kernel* of the control sequence and t' the time delay between signal and control fields [Fig. 3(a)]. Specifically, for the bipartite sequence of Fig. 1(e), the sensing kernel is

$$k(t) = \begin{cases} \sin[\Omega(\tau/2 - |t|)] & |t| < \tau/2 \\ 0 & |t| > \tau/2 \end{cases}. \tag{11}$$

In the frequency domain, the kernel is given by the transfer function $K(\omega) = |\mathrm{FT}[k(t)]|$,

$$K(w) = \frac{\sqrt{\frac{2}{\pi}}\Omega|\cos(\Omega\tau/2) - \cos(\omega\tau/2)|}{|\Omega^2 - \omega^2|}, \tag{12}$$

where FT is the Fourier transform. $K(\omega)$ for other sensing sequences, such as those using amplitude-shaped pulses, can be computed numerically using spin dynamics simulations [20]. Amplitude shaping will, however, always worsen time resolution, because qubit rotations are below the maximum possible Ω.

Figures 3(b) and 3(c) plot kernel profiles $k(t)$ and corresponding transfer functions $K(\omega)$ for several rotation angles $\alpha = \Omega\tau$ between 0° and 90°. Clearly, a smaller α leads to narrower kernels and, thus, an improved time

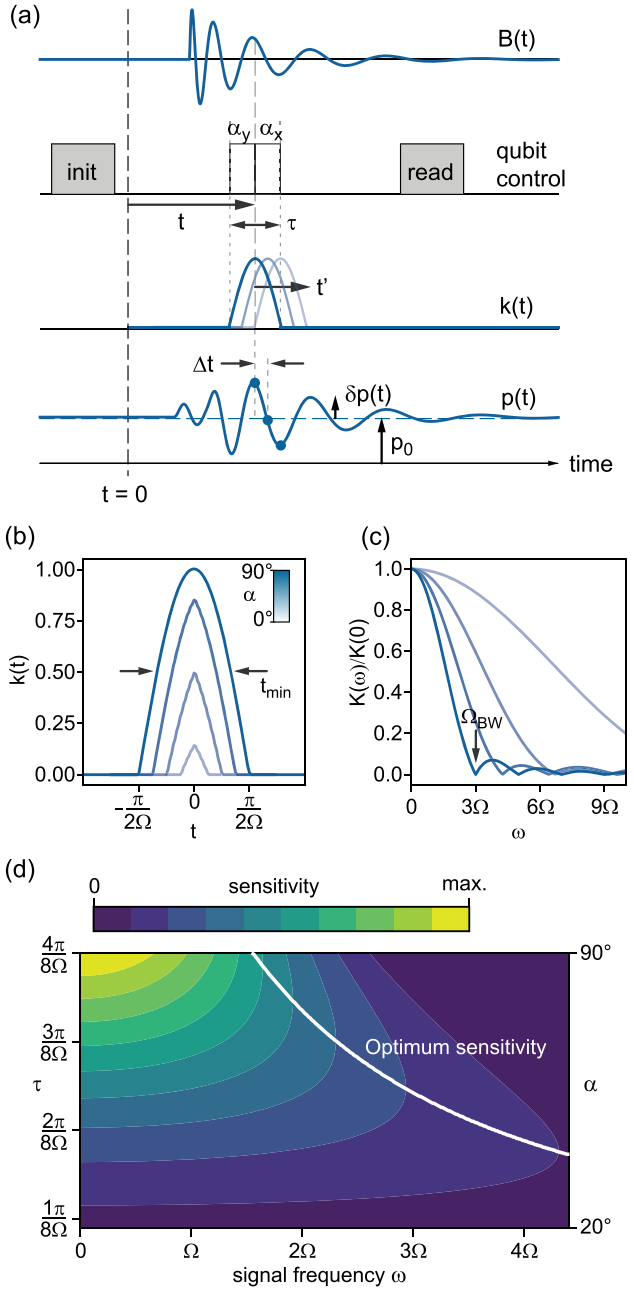

FIG. 3. Qubit output and sensing kernel. (a) Timing diagram. To sample the signal transient $B(t)$, the control sequence (second line) is stepped along t in increments of Δt. The output signal, given by state probability $p(t)$, is the convolution between $B(t)$ and the kernel $k(t)$ of the control sequence. Gray blocks represent initialization and readout of the qubit state, and white blocks represent the control rotations. (b) Kernel $k(t)$ for control rotation angles $\alpha = 22.5°$ (light blue), 45°, 67°, and 90° (dark blue). Kernels are computed using a lab-frame simulation of the spin evolution [20]. The time resolution $t_{\min}$ is defined by the full width at half maximum. (c) Normalized Bode plots $K(\omega)$ for the kernels shown in (b). The bandwidth Ω_{BW} is defined by the first root of $K(\omega)$. (d) Sensitivity $\eta \propto K(\omega)$ as a function of signal frequency ω and pulse duration τ at fixed Rabi frequency Ω. For dynamical signals $\omega > 0$, an optimum pulse duration exists where sensitivity is maximized (white curve).

resolution. Defining the time resolution $t_{\min}$ by the full width at half maximum of $k(t)$, we find for the bipartite control pulse that

$$t_{\min} := \tau\left(1 - \frac{\arcsin\frac{\sin\alpha}{2}}{\alpha}\right) \tag{13}$$

(See [20] for other possible definitions of $t_{\min}$). Specifically, $t_{\min} = \frac{2}{3}\tau = (2\pi/3\Omega)$ for $\alpha = 90°$, and $t_{\min} \approx \frac{1}{2}\tau = (\alpha/2\Omega)$ in the limit $\alpha \to 0$. Further, we can define a frequency bandwidth by the first root of the transfer function $K(\omega)$, given by

$$\Omega_{\mathrm{BW}} := \Omega\left(\frac{2\pi}{\alpha} - 1\right), \tag{14}$$

where $\Omega_{\mathrm{BW}} = 3\Omega$ for $\alpha = 90°$ [Fig. 3(c) and [20]].

For a given angular velocity Ω, shorter rotation angles $\alpha < 90°$ therefore provide a means to further improve the time resolution. The improvement is approximately $t_{\min} \propto \alpha$, and, correspondingly, for the bandwidth, $\Omega_{\mathrm{BW}} \propto \alpha^{-1}$. The improved time resolution, however, comes at the expense of a drastically lowered sensitivity, since $\eta \propto \alpha^2$ for small α [Eqs. (7) and (8)]. The sensitivity is further illustrated in Fig. 3(d), which plots η as a function of τ for arbitrary signal frequencies ω. An initial experimental demonstration of our technique is discussed in Ref. [21].

The apparent improvement of the time resolution beyond the QSL for short α [Eq. (13)] is in accordance with the interpretation of the uncertainty principle as defined by Eq. (1): the QSL reflects the minimum time required for transferring a quantum state to a *fully orthogonal* state. By reducing the orthogonality, thus not fully transferring the state, the time requirement shrinks therefore permitting a higher time resolution.

As a practical example, we consider the $S = 1$ spin system of a single nitrogen-vacancy center in diamond [22]. The NV center is a prototypical qubit sensor with a growing range of applications in materials science, physics, chemistry, and biology [23–28], including the study of dynamical excitations in these systems [29–31]. The NV center exhibits three spin energy levels $m_S = 0$ and $m_S = \pm 1$ and two allowed spin transitions with frequencies ω and ω', as depicted in Fig. 4(a). To form an effective two-level system, the ω (or ω') transition can be isolated by applying an axial bias field B_0 along the NV symmetry axis [Fig. 4(b)]. For driving fields Ω smaller than the frequency difference $|\omega' - \omega|$ between the $m_S = \pm 1$ levels [Fig. 4(c)], the excitation is selective and the other (ω' or ω) transition can be neglected.

Figure 4(d) shows the expected output probability p for a NV spin qubit as a function of Ω. The output probability is calculated using a laboratory-frame simulation of the spin dynamics, taking the full $S = 1$ nature of the NV center and the effect of counterrotating terms in the excitation pulses

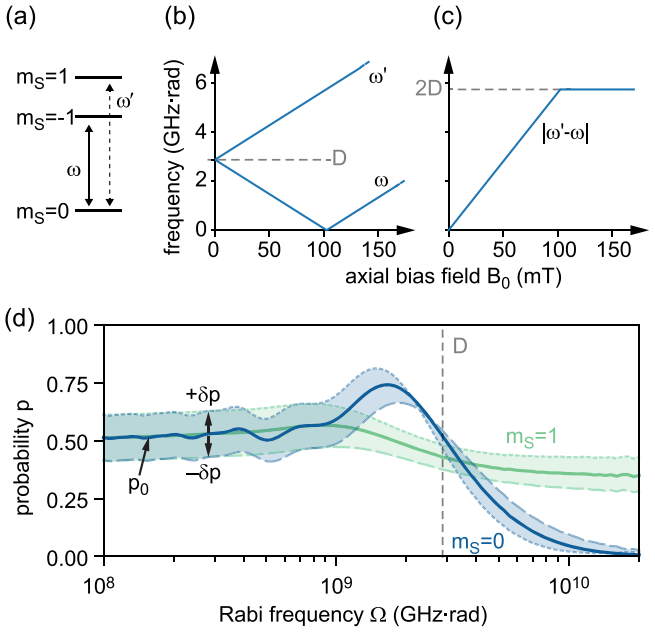

FIG. 4. Ultimate limits to time resolution for an NV probe qutrit. (a) NV spin energy levels and allowed transitions ω and ω'. (b) Scaling of transition frequencies ω and ω' with axial bias field B_0. $D = 2.87$ GHz is the zero-field splitting parameter. (c) Isolation of transition frequencies $|\omega' - \omega|$ as a function of B_0. The frequency difference saturates at two dimensions. (d) Numerical simulation of the state probability p as a function of driving frequency Ω. p_0 is the bias point and δp the probability change caused by the signal, see Eq. (6). At high $\Omega/2\pi > D$, the probability signal inverts and goes to zero for $\Omega \to \infty$ for preparation and measurement in the $m_S = 0$ basis (blue), but not in the $m_S = \pm 1$ (green) basis. For the simulation, a fixed value of $\delta\phi = 0.2$ was taken independent of Ω.

into account [20]. Two simulations are presented where the spin is either initialized and read out in the $m_S = 0$ state or in the $m_S = -1$ state, respectively.

First, we consider the $m_S = 0$ case. For moderate driving fields Ω that are safely smaller than any of the transition frequencies (ω, ω', $|\omega' - \omega|$), the output probability p is nearly independent of Ω and follows the theory of Eq. (7). On the other hand, for larger Ω, the output probability is modified due to strong driving effects—namely, Bloch-Siegert shifts and breakdown of the rotating-wave approximation [32–34]—and by spurious excitation of the ω' transition. Both effects are not accounted for by the basic theory of Eq. (7). Further, because the ω and ω' transitions lead to opposite signs in the phase ϕ_{eff}, the signal is completely canceled for very large $\Omega \gg |\omega' - \omega|$ [blue trace in Fig. 4(d)].

By contrast, when preparing and reading out the $m_S = -1$ spin state [green trace in Fig. 4(d)], the cancellation remains incomplete at any bias field. This provides a remedy to the $m_S = 0$ case. The incomplete cancellation is due to selection rules for qubit rotations: transitions are allowed between $m_S = 0$ and $m_S = \pm 1$, but forbidden between $m_S = -1$ and $m_S = +1$ states. Preparation and readout of $m_S = \pm 1$ are realized experimentally by slow, selective π rotations.

In summary, our work establishes limits to the temporal resolution reachable by a quantum sensor. We develop our discussion in the framework of the QSL, which is applied to the canonical sensing principle of Ramsey interferometry. We derive expressions for the coherent phase pickup during a generic sequence consisting of two phase-shifted control pulses and analyze the response regarding time resolution, frequency bandwidth, and sensitivity. We numerically simulate the expected phase response for the single spin of an NV center in diamond, taking the full $S = 1$ nature of the spin system and nonlinear driving effects into account. Beyond fundamental aspects in quantum metrology, our work has practical relevance for real-world applications of quantum sensors, such as the mapping of fast magnetization reversals in spintronic devices. These dynamics typically occur on timescales of a few nanoseconds [35]. For NV centers, $t_{\text{min}} \sim 1$ ns is reached, for example, using $\Omega/2\pi = 100$ MHz and $\alpha = 60°$ [Eq. (13)]. Such Rabi frequencies Ω are available using on-chip microwave delivery [33].

Acknowledgments—The authors thank John Abendroth, Joseph Renes, and Laura Alicia Völker for fruitful discussions. This work has been supported by Swiss National Science Foundation (SNSF) Project Grant No. 200020_212051/1 and by the European Research Council through ERC CoG 817720 (IMAGINE).

[1] H. P. Robertson, The uncertainty principle, Phys. Rev. **34**, 163 (1929).
[2] N. Bohr, The quantum postulate and the recent development of atomic theory, Nature (London) **121**, 580 (1928).
[3] L. Mandelstam, The uncertainty relation between energy and time in nonrelativistic quantum mechanics, J. Phys. (USSR) **9**, 249 (1945).
[4] S. Deffner and S. Campbell, Quantum speed limits: From Heisenberg's uncertainty principle to optimal quantum control, J. Phys. A **50**, 453001 (2017).
[5] N. Margolus and L. B. Levitin, The maximum speed of dynamical evolution, Physica (Amsterdam) **120D**, 188 (1998).
[6] G. Ness, A. Alberti, and Y. Sagi, Quantum speed limit for states with a bounded energy spectrum, Phys. Rev. Lett. **129**, 140403 (2022).
[7] L. B. Levitin and T. Toffoli, Fundamental limit on the rate of quantum dynamics: The unified bound is tight, Phys. Rev. Lett. **103**, 160502 (2009).
[8] G. Ness, M. R. Lam, W. Alt, D. Meschede, Y. Sagi, and A. Alberti, Observing crossover between quantum speed limits, Sci. Adv. **7**, eabj9119 (2021).
[9] Y. Zhang, W. Han, Y. Xia, J. Cao, and H. Fan, Quantum speed limit for arbitrary initial states, Sci. Rep. **4**, 4890 (2014).

[10] V. Giovannetti, S. Lloyd, and L. Maccone, Quantum limits to dynamical evolution, Phys. Rev. A **67**, 052109 (2003).
[11] K. Svozil, L. B. Levitin, T. Toffoli, and Z. Walton, Maximum speed of quantum gate operation, Int. J. Theor. Phys. **44**, 965 (2005).
[12] S. Lloyd, Ultimate physical limits to computation, Nature (London) **406**, 1047 (2000).
[13] S. Lloyd, Computational capacity of the universe, Phys. Rev. Lett. **88**, 237901 (2002).
[14] T. Caneva, M. M. T., Calarco, R. Fazio, S. Montangero, V. Giovannetti, and G. E. Santoro, Optimal control at the quantum speed limit, Phys. Rev. Lett. **103**, 240501 (2009).
[15] F. Campaioli, F. A. Pollock, F. C. Binder, L. Céleri, J. Goold, S. Vinjanampathy, and K. Modi, Enhancing the charging power of quantum batteries, Phys. Rev. Lett. **118**, 150601 (2017).
[16] M. P. Woods, R. Silva, G. Pütz, S. Stupar, and R. Renner, Quantum clocks are more accurate than classical ones, PRX Quantum **3**, 010319 (2022).
[17] C. L. Degen, F. Reinhard, and P. Cappellaro, Quantum sensing, Rev. Mod. Phys. **89**, 035002 (2017).
[18] J. M. Taylor, P. Cappellaro, L. Childress, L. Jiang, D. Budker, P. R. Hemmer, A.Yacoby, R. Walsworth, and M. D. Lukin, High-sensitivity diamond magnetometer with nanoscale resolution, Nat. Phys. **4**, 810 (2008).
[19] In general, the initial and readout bases may be different, but for simplicity and without loss of generality, we assume them to be the same [17].
[20] See Supplemental Material at http://link.aps.org/supplemental/10.1103/PhysRevLett.133.210802 for proof of optimality of pulse parameters.
[21] K. Herb, L. A. Völker, J. M. Abendroth, N. Meinhardt, L. van Schie, P. Gambardella, and C. L. Degen, Quantum magnetometry of transient signals with a time resolution of 1.1 nanoseconds, arXiv:2411.05542.
[22] M. W. Doherty, N. B. Manson, P. Delaney, F. Jelezko, J. Wrachtrup, and L. C. Hollenberg, The nitrogen-vacancy colour centre in diamond, Phys. Rep. **528**, 1 (2013).
[23] R. Schirhagl, K. Chang, M. Loretz, and C. L. Degen, Nitrogen-vacancy centers in diamond: Nanoscale sensors for physics and biology, Annu. Rev. Phys. Chem. **65**, 83 (2014).
[24] J. F. Barry, M. J. Turner, J. M. Schloss, D. R. Glenn, Y. Song, M. D. Lukin, H. Park, and R. L. Walsworth, Optical magnetic detection of single-neuron action potentials using quantum defects in diamond, Proc. Natl. Acad. Sci. U.S.A. **113**, 14133 (2016).
[25] E. Janitz, K. Herb, L. A. Volker, W. S. Huxter, C. L. Degen, and J. M. Abendroth, Diamond surface engineering for molecular sensing with nitrogen-vacancy centers, J. Mater. Chem. C **10**, 13533 (2022).
[26] G. Petrini, G. Tomagra, E. Bernardi, E. Moreva, P. Traina, A. Marcantoni, F. Picollo, K. Kvaková, P. Cígler, I. P. Degiovanni, V. Carabelli, and M. Genovese, Nanodiamond–quantum sensors reveal temperature variation associated to hippocampal neurons firing, Adv. Sci. **9**, 2202014 (2022).
[27] A. Finco and V. Jacques, Single spin magnetometry and relaxometry applied to antiferromagnetic materials, APL Mater. **11**, 100901 (2023).
[28] J. Rovny, S. Gopalakrishnan, A. C. B. Jayich, P. Maletinsky, E. Demler, and N. P. d. Leon, New opportunities in condensed matter physics for nanoscale quantum sensors, arXiv:2403.13710.
[29] T. V. der Sar, F. Casola, R. Walsworth, and A. Yacoby, Nanometre-scale probing of spin waves using single electron spins, Nat. Commun. **6**, 7886 (2015).
[30] C. S. Wolfe, S. A. Manuilov, C. M. Purser, R. Teeling-Smith, C. Dubs, P. C. Hammel, and V. P. Bhallamudi, Spatially resolved detection of complex ferromagnetic dynamics using optically detected nitrogen-vacancy spins, Appl. Phys. Lett. **108**, 232409 (2016).
[31] B. B. Zhou, P. C. Jerger, K. H. Lee, M. Fukami, F. Mujid, J. Park, and D. D. Awschalom, Spatiotemporal mapping of a photocurrent vortex in monolayer MoS_2 using diamond quantum sensors, Phys. Rev. X **10**, 011003 (2020).
[32] F. Bloch and A. Siegert, Magnetic resonance for nonrotating fields, Phys. Rev. **57**, 522 (1940).
[33] G. D. Fuchs, V. V. Dobrovitski, D. M. Toyli, F. J. Heremans, and D. D. Awschalom, Gigahertz dynamics of a strongly driven single quantum spin, Science **326**, 1520 (2009).
[34] P. Kairys, J. C. Marcks, N. Delegan, J. Zhang, D. D. Awschalom, and F. J. Heremans, Quantifying the limits of controllability for the nitrogen-vacancy electron spin defect, arXiv:2309.03120.
[35] M. Baumgartner, K. Garello, J. Mendil, C. O. Avci, E. Grimaldi, C. Murer, J. Feng, M. Gabureac, C. Stamm, Y. Acremann, S. Finizio, S. Wintz, J. Raabe, and P. Gambardella, Spatially and time-resolved magnetization dynamics driven by spin-orbit torques, Nat. Nanotechnol. **12**, 980 (2017).